International Journal of Heat and Mass Transfer 52 (2009) 124–132

Contents lists available at ScienceDirect

International Journal of Heat and Mass Transfer

journal homepage: www.elsevier.com/locate/ijhmt

Numerical investigation of non-isothermal phase change phenomena in vertical Bridgman crystal growth

Jie Liu, Wen-Qiang Lu *

College of Physical Sciences, Graduate University of Chinese Academy of Sciences, Beijing 100049, PR China

ARTICLE INFO

Article history:
Received 18 February 2008
Received in revised form 3 June 2008
Available online 12 August 2008

Keywords:
Non-isothermal phase change phenomena
Double-diffusive convection
Vertical Bridgman crystal growth

ABSTRACT

The non-isothermal phase change phenomena during the vertical Bridgman growth process for HgCdTe are numerically investigated using an interface capturing finite element scheme. The influence of the growth parameters such as *Bi*, *Ste*, *U* and the flow parameters including Gr_T and Gr_S on the non-isothermal phase change phenomena are obtained. Some new features about the melt/crystal interface shape, the temperature field near the interface and the flow field are revealed by comparing the non-isothermal phase change with the isothermal phase change. Furthermore, the comparison of the non-isothermal interfacial characteristics between the pure diffusion, the natural convection and the double-diffusive convection is made and the obvious differences are presented.

1. Introduction

II–VI compound semiconductor materials, such as HgCdTe, HgZnTe and CdZnTe, are composed of two, three or four IIB elements such as Zn, Cd and Hg, and VIA elements such as S, Se and Te in the periodic table of the elements. Many applications of these materials are being developed for new kinds of instruments such as lasers, infrared detectors and imaging instruments because of their special electrical, optical and photoelectrical properties. Therefore, significant research has been made focusing on the pure crystal growth process for these materials in the recent years [1–5].

The vertical Bridgman method (VBM) was firstly developed in 1925. Now it is one of the best and popular techniques for the growth of semiconductor crystals. A schematic diagram of a typical vertical Bridgman growth system is shown in Fig. 1(a). This technique has the advantage of steady temperature fields, controllable temperature gradients and purification. The method can yield pure crystals of large sizes by controlling the boundary conditions of heat and mass transfer. Therefore, it is widely used to produce II–VI compound semiconductor crystals. As we all know that the interface shape during the crystal growth process significantly affects the final crystal quality. Plane, stable interfaces are good for high-quality crystal growth; however, in practice, planer interfaces are not easy to obtain. In the phase diagram of HgCdTe [6], the solidus and liquidus lines are far apart, so it is thinkable that there is remarkable concentration segregation of the solvent HgTe from the crystal into the melt at the interface. This segregation makes it difficult to grow large, uniform, high-quality HgCdTe crystals because of multi-elements non-isothermal phase change. Therefore, it is very important to comprehend interfacial characteristics such as interface shape, concentration segregation, melting temperature, and non-isothermal phase change which occur at the melt/crystal interface.

Since II–VI semiconductor materials are not transparent and the practical growth process are implemented at high temperatures and other difficult experimental conditions, visual observation of the phenomena and measurements of temperature, concentration and velocity fields during the growth process are almost impossible. Numerical simulations have special significance in this research field. Capper et al. [7] investigated the shape of the melt/crystal interface by rapidly quenching HgCdTe crystals using VBM. They showed that the interface is a paraboloid with the center lower than the edges. Wang et al. [8] investigated the effects of growth speed on the interface shape by pulling. Their results illustrated that the concave paraboloid becomes more concave with higher growth speeds. Hong and Wei [9] numerically studied steady state Bridgman growth of a CdTe crystal with two ampoule configurations. Their results revealed that although the two ampoule configurations were quite different, they had similar influence on the melt/crystal interface shape with the undesirable concave interface. A numerical simulation was carried by Lan and Ting [10] to study the interface morphology during Bridgman crystal growth illustrated the effects of growth speed, ambient temperature profile and ampoule design. Liu and Chen [11] numerically studied the effects of gravity on the interface in a horizontal Bridgman growth system. The strong convection in the melt can lead to a concave interface in the crystal, but the interface becomes flat when the gravity is small enough. Wei et al. [12] analyzed the influence of the pulling rate and ambient temperature distribution

* Corresponding author. Tel.: +86 10 88256277; fax: +86 10 81717831.
E-mail address: luwq@gucas.ac.cn (W.-Q. Lu).

0017-9310/$ - see front matter © 2008 Elsevier Ltd. All rights reserved.
doi:10.1016/j.ijheatmasstransfer.2008.06.017

Nomenclature

A	aspect ratio $A = H/R$
Bi	Biot number
C	dimensionless solute concentration C^*/C_0^*
C^*	solute concentration (mole fraction)
C_0^*	initial solute concentration (mole fraction)
C_p	specific heat capacity at constant pressure (J/°C g)
D	solute diffusivity (cm^2/s)
Gr_S	solutal Grashof number
Gr_T	thermal Grashof number
g	gravitational acceleration (cm/s^2)
H	height of the enclosure (cm)
k	the thermal conductivity (W/K cm)
K_0	segregation coefficient of CdTe
Pr	Prandtl number
r, z	dimensionless radial and axial coordinates, $r = r^*/R$, $z = z^*/R$
$\hat{r}, \hat{z}$	dimensionless radial and axial coordinates in the transformed coordinate system
R	radius of the enclosure (cm)
Sc	Schmidt number
Ste	Stefan number
T	dimensionless temperature $(T^* - T_L^*)/(T_H^* - T_L^*)$
T^*	temperature (°C)
T_H, T_L	the dimensionless highest and lowest temperature of the ambient temperature
U	dimensionless pulling rate
U^*	the pulling rate (cm/s)
u_r, u_z	dimensionless radial and axial velocity
u_r^*, u_z^*	radial and axial velocity (cm/s)
ΔH	the latent heat of solidification (J/g)

Greek symbols

α	thermal diffusive coefficient (cm^2/s)
β_S	coefficient of solutal expansion ((mole faction CdTe)$^{-1}$)
β_T	coefficient of thermal expansion (°C^{-1})
ν	kinematic viscosity (cm^2/s)
ρ	density (g/m^3)
τ	ratio of melt and crystal thermal conductivities
ψ	dimensionless stream-function
ψ^*	stream-function (cm^3/s)
ω	dimensionless vorticity
ω^*	vorticity (s^{-1})

Superscript

$*$	dimensional quantities

Subscripts

c	crystal
f	furnace
m	melt
S	solutal
T	thermal

on the melt/crystal interface for Bridgman growth of CdTe. The results show that a lower growth rate produces a flatter interface. Increasing the temperature gradients has also proved effective for improving the interface. Wang et al. [13] brought forward the simplified formula of heat transfer coefficient between the furnace and the ampoule under the condition of the three regions temperature design of furnace. Based on this formula and its modified form, Liu et al. [2,3] used the finite difference method (FDM) to analyze the influence of the accelerated crucible rotation technique (ACRT) on the crystal growth by VBM. Bourret et al. [14–16] studied the variation of the phase change interface position with the time, solute concentration redistribution and the melting temperature after the system reached steady state, and so captured one-dimensional non-isothermal phase change phenomena. On the basis of the axial solute concentration redistribution during the HgCdTe growth process, Wang et al. [17] studied the optimal expression of the initial growth rate to lead to decreasing the length of the initial transient region and increasing the length of the steady growth region. Yeckel and Derby [18] performed the theoretical simulations of VB growth of cadmium zinc telluride and got the effects of the ACRT. Kawaguchi et al. [19] simulate the contributions of CCRT, ACRT, thermal and solutal gradients to the convection in the melt during the growth of CdZnTe crystals by the vertical gradient freezing (VGF) method.

As far as authors' knowledge is concerned, crystal growth studies have been mainly done by material's science researchers using experiments or numerical methods. However, the physical processes during crystal growth are very complex; they include multi-elements heat and mass transfer, non-isothermal phase change and double-diffusive convection. The thermophysical analyses of the processes are insufficient, especially non-isothermal phase change phenomena. There have been few studies of factors affecting interfacial characteristics of the non-isothermal phase change phenomena during growth process of II–VI compounds. Shi et al. [20] analyzed the effects of the Bridgman process parameters and the double-diffusive convection in the melt on the melt/crystal interface shape and the solute distribution for the II–VI semiconductor material based on the isothermal phase change. Liu and Lu [21,22] systematically studied one- and two-dimensional non-isothermal phase change phenomena without considering the convection in the melt. The research about two-dimensional non-isothermal phase change phenomena with flow and the influence of double-diffusive convection on the non-isothermal phase change have not been dealt with in the literature. So the current work uses an interface capturing finite element scheme to analyze the two-dimensional non-isothermal phase change phenomena with flow during the II–VI compound crystal growth.

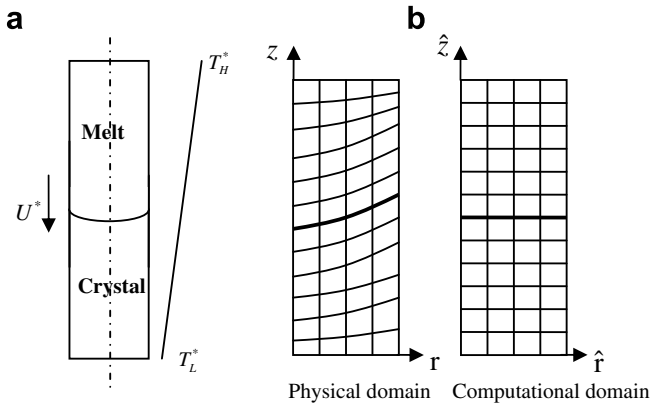

Fig. 1. Schematic diagram of vertical Bridgman growth (a) and sample finite element mesh geometry (b).

2. Physical model and boundary conditions

The calculating model of vertical Bridgman method in the crystal growth is schematically shown in Fig. 1(a). The material is in a furnace with a linear temperature gradient and a pulling down rate, U^*. So the melt is corresponding to the high-temperature zone

while the solidified crystal is in the low-temperature zone. During the downward pulling process, the melt is continuously solidified to form the crystal as it releases heat to the ambient. A typical Bridgman crystal growth process can be divided into initial transient region, steady growth region and final transient region. In the initial and final transient region, the flow and solute distribution near the interface in the melt are not stable, which leads to nonuniform solute distribution in the crystal. In the steady growth region, the flow and solute distribution in the melt tend to be stable, so the crystal composition is also stable. The steady growth region should be extended to get more usable crystal. This paper puts focus on the steady grow region with the coordinate system shown in Fig. 1(b). The solutal diffusion in the crystal can be neglected because of low solutal diffusivity and the crystal growth speed is assumed to be equal to the pulling rate.

The governing equations were written using a vorticity and stream function formulation. The stream function, ψ^*, and the vorticity, ω^*, are defined as:

$$u_r^* = \frac{1}{r^*}\frac{\partial \psi^*}{\partial z^*}, \quad u_z^* = -\frac{1}{r^*}\frac{\partial \psi^*}{\partial r^*} \tag{1}$$

$$\omega^* = \frac{\partial u_r^*}{\partial z^*} - \frac{\partial u_z^*}{\partial r^*} \tag{2}$$

The equations for the vorticity, stream function, energy conservation and species conservation in dimensionless form are:

$$\frac{1}{r}\frac{\partial \psi}{\partial z}\frac{\partial \omega}{\partial r} - \frac{1}{r}\frac{\partial \psi}{\partial r}\frac{\partial \omega}{\partial z} - \frac{\omega}{r^2}\frac{\partial \psi}{\partial z} = \left(\frac{\partial^2 \omega}{\partial r^2} + \frac{1}{r}\frac{\partial \omega}{\partial r} + \frac{\partial^2 \omega}{\partial z^2} - \frac{\omega}{r^2}\right) - Gr_T\frac{\partial T}{\partial r} - Gr_S\frac{\partial C}{\partial r} \tag{3}$$

$$\frac{\partial^2 \psi}{\partial r^2} + \frac{\partial^2 \psi}{\partial z^2} - \frac{1}{r}\frac{\partial \psi}{\partial r} = r\omega \tag{4}$$

$$\frac{1}{r}\frac{\partial \psi}{\partial z}\frac{\partial T}{\partial r} - \frac{1}{r}\frac{\partial \psi}{\partial r}\frac{\partial T}{\partial z} = \frac{1}{Pr}\left(\frac{\partial^2 T}{\partial r^2} + \frac{1}{r}\frac{\partial T}{\partial r} + \frac{\partial^2 T}{\partial z^2}\right) \tag{5}$$

$$\frac{1}{r}\frac{\partial \psi}{\partial z}\frac{\partial C}{\partial r} - \frac{1}{r}\frac{\partial \psi}{\partial r}\frac{\partial C}{\partial z} = \frac{1}{Sc}\left(\frac{\partial^2 C}{\partial r^2} + \frac{1}{r}\frac{\partial C}{\partial r} + \frac{\partial^2 C}{\partial z^2}\right) \tag{6}$$

where C represents the CdTe concentration. The boundary conditions in dimensionless form are:

$$\text{Top}: \ T = 1, \quad \frac{\partial C}{\partial z} = ScU(1-K_0)C, \quad \psi = -\frac{1}{2}Ur^2, \quad \omega = 0 \tag{7}$$

$$\text{Bottom}: \ T = 0, \quad \frac{\partial C}{\partial z} = 0, \quad \psi = -\frac{1}{2}Ur^2, \quad \omega = 0 \tag{8}$$

$$\text{Sidewall}: \ -\frac{\partial T}{\partial r} = Bi_{m,c}(T_f - T), \quad \frac{\partial C}{\partial r} = 0, \quad \psi = -\frac{1}{2}U\left(\frac{1}{A}\right)^2, \quad \omega = \frac{\partial}{\partial r}\left(\frac{1}{r}\frac{\partial \psi}{\partial r}\right) \tag{9}$$

$$\text{Centerline}: \ \frac{\partial T}{\partial r} = \frac{\partial C}{\partial r} = 0, \quad \psi = \omega = 0 \tag{10}$$

$$\text{Interface}: \ T_m = 0.5 + 0.2\times C - 0.017\times C^2, \quad \left.\frac{\partial T}{\partial n}\right|_c = \tau\left.\frac{\partial T}{\partial n}\right|_m + \frac{PrU}{Ste}, \quad -\frac{\partial C}{\partial z} = ScU(1-K_0)C, \quad \psi = -\frac{1}{2}Ur^2, \quad \omega = \frac{\partial}{\partial z}\left(\frac{1}{r}\frac{\partial \psi}{\partial z}\right) + \frac{\partial}{\partial r}\left(\frac{1}{r}\frac{\partial \psi}{\partial r}\right) \tag{11}$$

where $Gr_T = \frac{g\beta_T \Delta T^* R^3}{\nu^2}$, $Gr_S = \frac{g\beta_S C_0^* R^3}{\nu^2}$, $Pr = \nu/\alpha$, and $Ste = C_{p,m}\Delta T/\Delta H$. In these equations, the lengths were nondimensionalized by R, which is the radius of the computational region, the stream function by νR, the vorticity by ν/R^2, $(T^* - T_L^*)$ by $\Delta T^* (= T_H^* - T_L^*)$ and the solute concentration by $C_0^* (= 0.15)$ which represents the initial solute concentration. In the calculations, the dimensionless ambient temperature $T_f(z) = T_L + (T_H - T_L)z$ is chosen where T_H and T_L is the highest and lowest temperature at the two end of the furnace. The Biot number in Eq. (9) is defined as $Bi_{m,c} \equiv hR/k_{m,c}$ [23]. The dimensionless melting temperature $T_m = 0.5 + 0.2\times C - 0.017\times C^2$ (in Eq. (11)) is calculated from the formula according to the phase diagram in Ref. [2].

3. Numerical method

3.1. Grid discretization and coordinate transformation

The grid distribution for the calculations is shown in Fig. 1(b). In the original coordinate system, the meshes were irregular quadrilaterals due to the concave interface between the melt and the crystal. The coordinates were then transformed to a rectangular mesh. The concave interface was transformed to a horizontal surface in the transformed coordinate system with the interface position in the middle of the computational region.

The relationships between the transformed coordinates and the original coordinates are [24]

$$\text{Crystal}: \ \hat{r} = r, \quad \hat{z} = \frac{zH}{2h}(r) \tag{12}$$

$$\text{Melt}: \ \hat{r} = r, \quad \hat{z} = \left[1 - \frac{H-z}{2(H-h(r))}\right]H \tag{13}$$

where $h(r)$ is the interface position in the original coordinates. The melt/crystal interface is at $\hat{z} = 0.5H$ in the transformed coordinate system.

The corresponding differential relations are:

$$\begin{cases} dr = d\hat{r} \\ dz = \frac{2ac}{H}d\hat{r} + \frac{2b}{H}d\hat{z} \end{cases} \tag{14}$$

$$\begin{cases} \frac{\partial}{\partial r} = \frac{\partial}{\partial \hat{r}} - \frac{ac}{b}\frac{\partial}{\partial \hat{z}} \\ \frac{\partial}{\partial z} = \frac{H}{2b}\frac{\partial}{\partial \hat{z}} \end{cases} \tag{15}$$

crystal: $a = \hat{z}, \ b = h(\hat{r}), \ c = h'(\hat{r}) = \frac{\partial h}{\partial \hat{r}}$,
melt: $a = H - \hat{z}, \ b = H - h(\hat{r}), \ c = h'(\hat{r}) = \frac{\partial h}{\partial \hat{r}}$.

3.2. Finite element scheme in transformed coordinates

In the transformed coordinates, the discretized elements are four-node rectangular elements (see Fig. 1(b)). Four-node rectangular elements can use a bilinear function $\Phi = b_1 + b_2\xi + b_3\eta + b_4\xi\eta$ to construct the finite element equations. The finite element scheme had been extended to the moving phase change interface problem using rectangular meshes in the transformed coordinates. The governing equations are solved numerically by the finite element scheme. An iterative scheme was used to capture the moving phase change interface. The implicit Euler backward scheme was used to discretize the time derivative terms. The variable band matrix equations were solved using Gauss elimination.

3.3. Iterative scheme for moving phase change interface

The moving phase change interface was captured using the following algorithm.

(1) Assume that the initial horizontal interface is at $z = 5$, $h^1(r) = h^1(\hat{r}) = 55$, $\frac{dh^1}{dr} = \frac{dh^1}{d\hat{r}} = 0$. Then generate the elements in the transformed coordinate system.

(2) Solve the governing equations in the transformed coordinate system and get the interfacial values of the solutal concentration C.
(3) Calculate $h^{n+1}(\hat{r})$ where the temperature is equal to T_m by interpolating in the axial direction.
(4) If the values of $h^{n+1}(\hat{r})$ satisfy $|\frac{h^{n+1}(\hat{r})-h^n(\hat{r})}{h^n(\hat{r})}| \leqslant \varepsilon = 10^{-5}$, then $h^{n+1}(\hat{r})$ is the desired interfacial position. If the error between $h^{n+1}(\hat{r})$ and $h^n(\hat{r})$ does not satisfy the required precision, a relaxation step is used to get a new $h^{n+1}(\hat{r})$, the coordinate transform coefficients in Eqs. (14) and (15) are recalculated and the algorithm returns to step (2).
(5) Output the required results.

4. Results and discussion

During the crystal growth process using VBM, the interface shape and melting temperature are affected by many parameters, such as *Bi*, *Ste*, *U*. The non-isothermal phase change which occurs at the interface will also change the interfacial characteristics and the flow field in the melt comparing with the isothermal phase change. The model was used to investigate the effects of such parameters and get some new features of the non-isothermal phase change.

The physical properties of HgCdTe and operating parameters were listed in Tables 1 [23] and 2. The calculational parameters were chosen as $Pr = 0.1$, $Sc = 19.6$, $Bi_c = 40$, $Ste = 1.0$, $U = 0.1$, $A = 10$ and $Gr_T = 1.0 \times 10^6$.

The numerical method has been employed by Shi et al. [20] to study the double-diffusive convection in the melt during the isothermal phase change Bridgman process and some reasonable results have been obtained. To test the grid independence of the scheme, the solutions have been obtained on the meshes of 41×201, 51×251 and 61×261, respectively. Fig. 2 shows that the results of different mesh are fitted well, so the mesh 51×251 is chosen in the following calculation.

4.1. Effects of growth parameters on the non-isothermal phase change phenomena

4.1.1. The basic calculating results of interfacial characteristics

Fig. 2 also illustrates the interface is concave to the crystal because the thermal conductivity in the melt is greater than that in the crystal ($k_m > k_c$) and the complex heat transfer process occurs at the interface and the wall. Fig. 3(a) shows that the CdTe concentration near the wall is higher than that near the centerline, this indicates the HgTe is segregated into the melt and concentrated

Table 1
Physical properties of HgCdTe [23]

Physical property	Symbol (Unit)	Value
Thermal conductivity of melt	k_m (W/K cm)	1.96×10^{-2}
Thermal conductivity of crystal	k_c (W/K cm)	2.91×10^{-3}
Density of melt	ρ_m (g/cm^3)	7.55
Density of crystal	ρ_c (g/cm^3)	7.63
Specific heat of melt	$c_{p,m}$ (J/K g)	0.257
Specific heat of crystal	$c_{p,c}$ (J/K g)	0.177
Latent heat of solidification	ΔH (J/g)	130
Diffusion of CdTe in melt	D (cm^2/s)	5.5×10^{-5}
Segregation coefficient of CdTe	K_0	2.7
Kinematic viscosity	v (cm^2/s)	1.08×10^{-3}

Table 2
Operating parameters

Parameter	Unit	Value
The pulling rate	cm/s	4.32×10^{-4}
Height of the enclosure	cm	2.5
Radius of the enclosure	cm	0.25
Temperature at the hot end	°C	920
Temperature at the cold end	°C	420
Initial CdTe concentration	Mole fraction	0.15

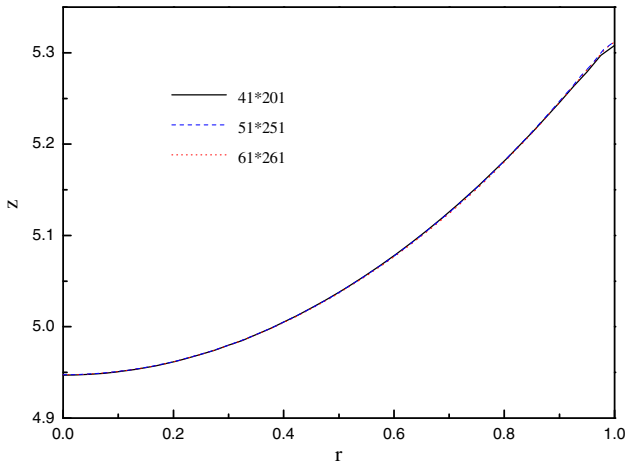

Fig. 2. Comparison of the results for different mesh schemes: the non-isothermal phase change interface position.

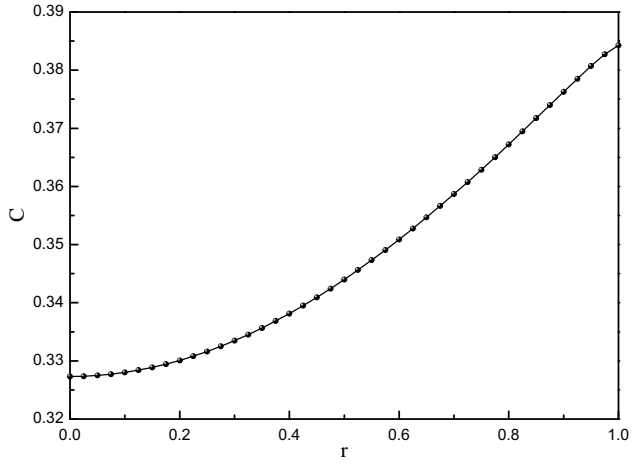

(a) The solute distribution, CdTe, at the interface

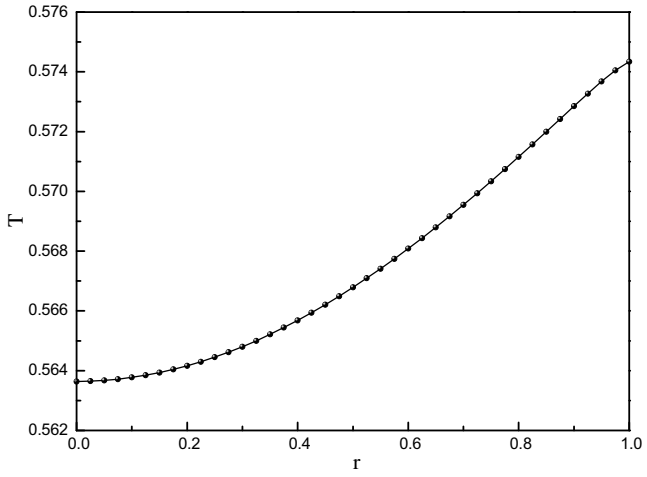

(b) The melting temperature

Fig. 3. Basic calculating results of interfacial characteristics.

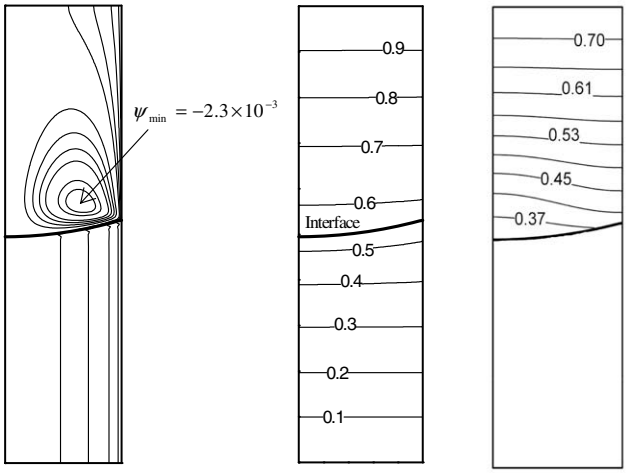

(a) Flow field (b) Temperature field (c) Solutal field

Fig. 4. Flow, temperature and solutal fields with the non-isothermal phase change phenomena.

at the centerline. Fig. 3(b) depicts the melting temperature correspondingly varies from the centerline to the wall at the phase change interface since the solute concentration varies radially.

Fig. 4 illustrates the predicated flow, temperature and solutal fields with the natural convection in the melt. The flow field in Fig. 4(a) shows a clockwise vortex exists for the given boundary conditions near the interface in the melt due to thermal buoyancy in the natural convection. However, the thermal field is scarcely affected by the natural convection due to the large thermal diffusivity (Fig. 4(b)). Because the solutal diffusivity is small, the natural convection in the melt strongly affects the solute distribution. Fig. 4(c) shows that the solute is well mixed by the vortex and the iso-concentration lines are tilting down near the interface.

4.1.2. Effects of Biot number

The effects of Bi_c on the interface shape and melting temperature are shown in Fig. 5. The heat transfer between the system and the ambient is enhanced with increasing Bi_c. As a result, the interface position moves upward along the wall (Fig. 5(a)), with its shape remaining essentially unchanged. The melting temperature at the interfaces correspondingly rises a little as the interface position changes (Fig. 5(b)).

4.1.3. Effects of growth speed U

The growth speed affects the quantity of solvent segregated from the crystal and the release of latent heat, which influence the interface shape, the solute distribution and the melting temperature. Fig. 6 shows more solvent (HgTe) segregates into the melt and concentrates towards the centerline as the growth speed

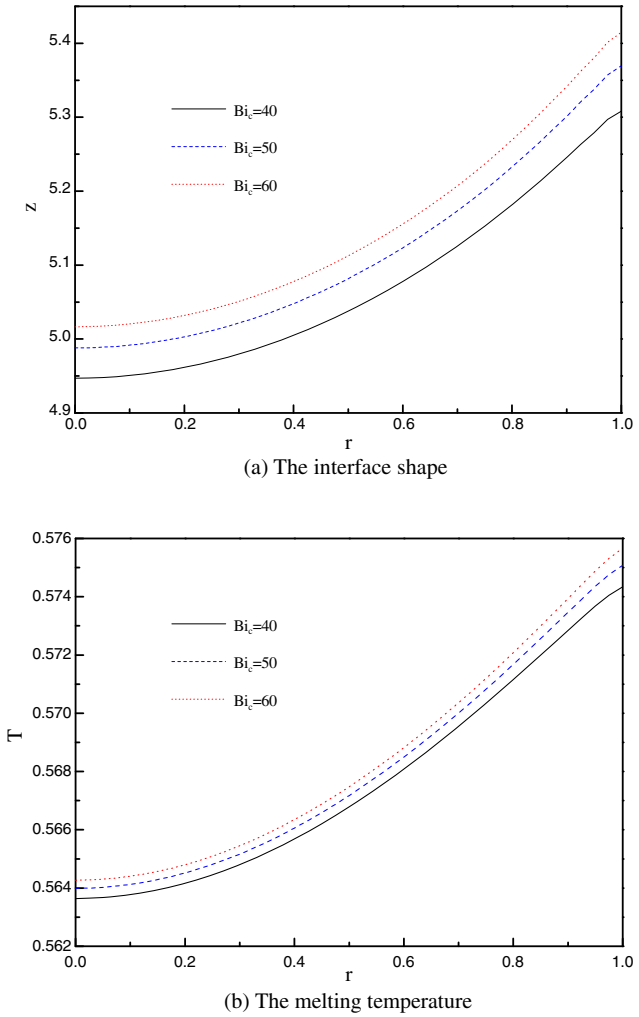

(a) The interface shape

(b) The melting temperature

Fig. 5. Effects of the Bi_c on the interface shape (a) and the melting temperature at the interface (b).

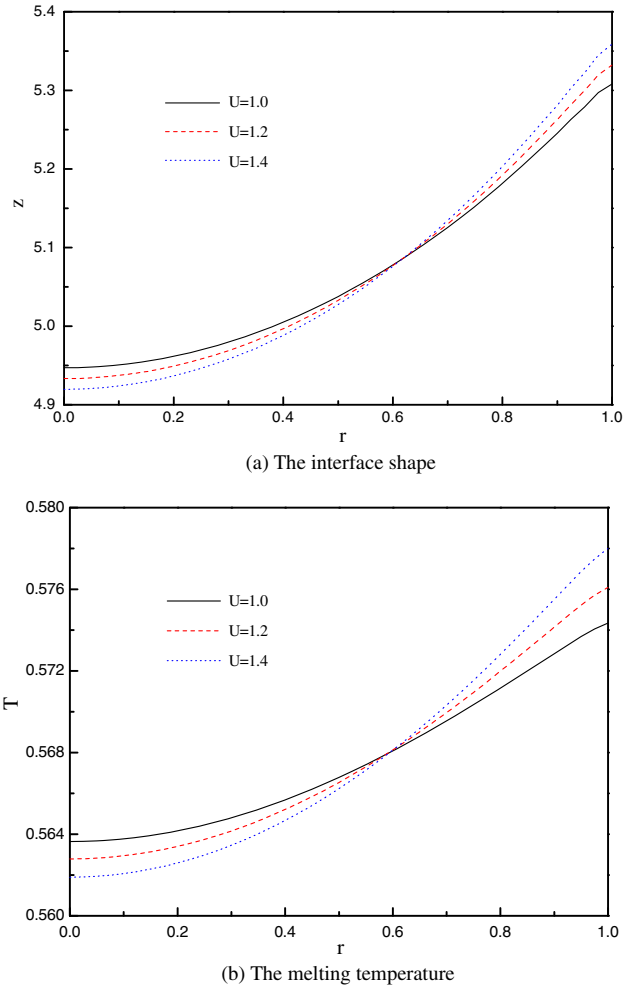

(a) The interface shape

(b) The melting temperature

Fig. 6. Effects of growth speed on the interface shape (a) and the melting temperature at the interface (b).

increases, so the temperature near the centerline is lower for lower solutal concentration. But more latent heat is released which cannot be immediately transferred to the ambient with a fixed ambient temperature and heat exchange coefficient. So interfacial temperature varies rapidly and the temperature difference between the wall and the centerline increases (Fig. 6(b)). Correspondingly, the interface depth (the difference of the interface position between the centerline and the wall) increases and the interface position near the centerline drops (Fig. 6(a)).

4.1.4. Effects of Ste number

Fig. 7 shows that the interface position near the centerline is lowered as the Stefan number increasing which means that the interface depth increases with increasing ΔT. However, the melting temperature at the interface is almost the same due to the constant growth speed and similar interface shape.

4.1.5. Effects of thermal Grashof number

The thermal Grashof number varies with the ambient temperature field while the thermal properties (β_T, ν) of the materials are kept constant. If the thermal Grashof number decreases, the temperature difference (ΔT) between the hot and cold ends will decrease which means smaller temperature gradients. The flow and heat transfer are enhanced for the larger thermal buoyancy. Fig. 8 shows the effect of increasing Gr_T: descending of the melting temperature and corresponding variation of the interfacial shape.

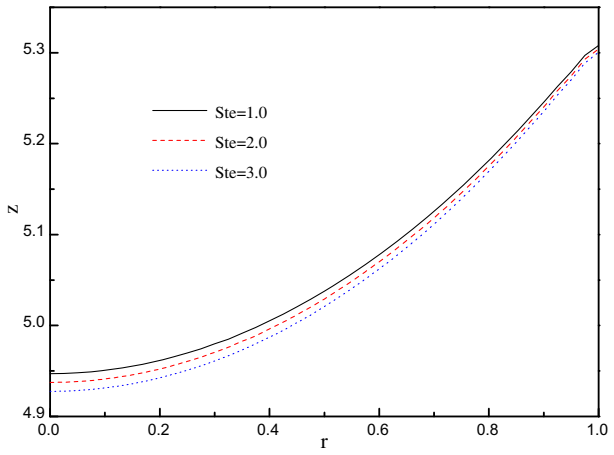

(a) The interface position

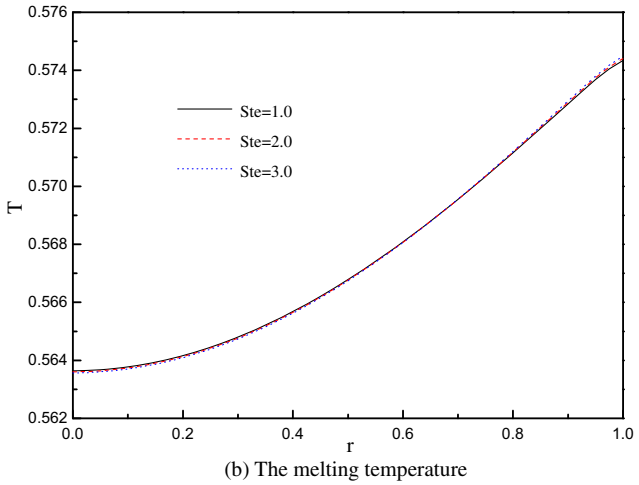

(b) The melting temperature

Fig. 7. Effects of the Stefan number on the interface shape (a) and the melting temperature at the interface (b).

4.2. The comparison between the non-isothermal phase change and isothermal phase change

The melting temperature in isothermal phase change is assumed to be uniform ($T_m = 0.5$). Other parameters are chosen as

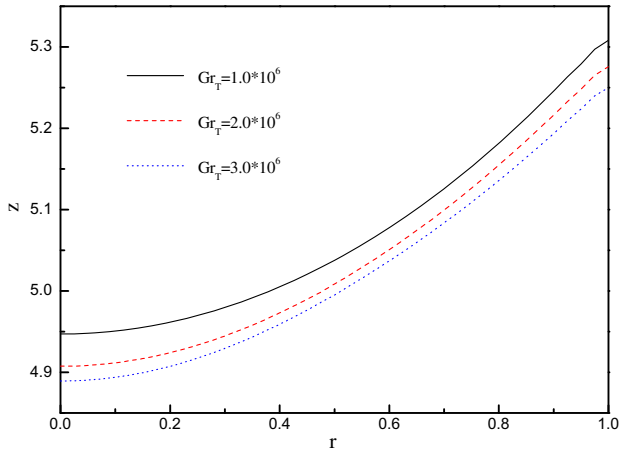

(a) The interface shape

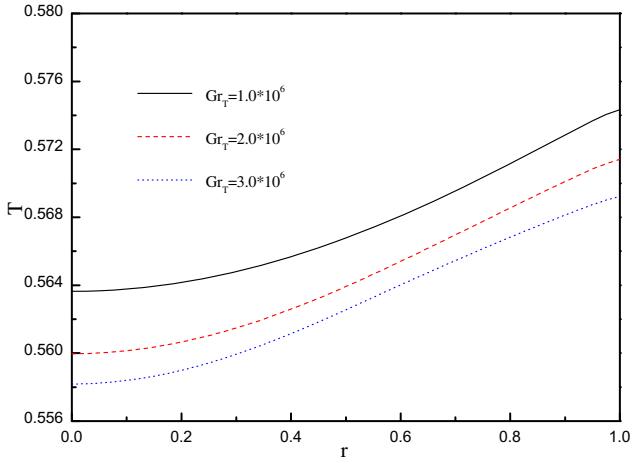

(b) The melting temperature

Fig. 8. Effects of Gr_T on the interface shape (a) and the melting temperature at the interface (b).

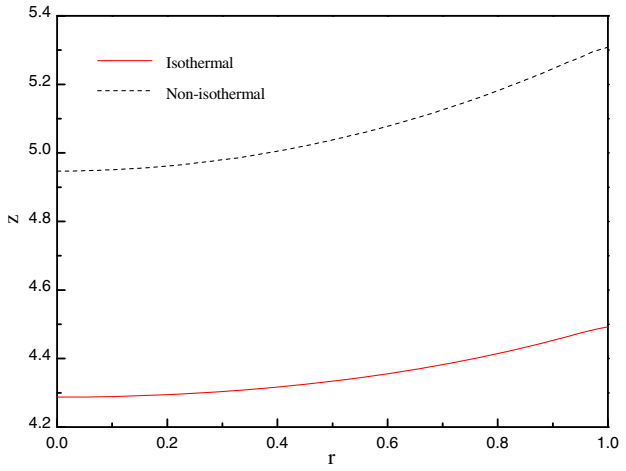

Fig. 9. The comparison of the interface shape between the non-isothermal and isothermal phase change.

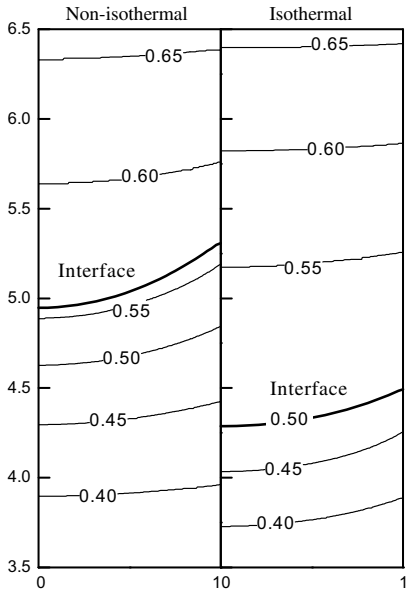

Fig. 10. The comparison of the temperature field (z = 3.5–6.5) between the non-isothermal and isothermal phase change.

the same as those in Section 4.1.1. The numerical results of the comparison between the isothermal and non-isothermal phase change show as follows.

4.2.1. The comparison of the interface shape

Fig. 9 shows the comparison of the interface shape between the non-isothermal phase change and isothermal phase change. Apparently, the melting temperature in the non-isothermal phase change (Fig. 3(b)) is greater than that in the isothermal phase change (T_m = 0.5). As a result, the interface position moves upward correspondingly in order to keep the approximately same amount of heat flux exchanged with the ambient temperature. It can be seen that the non-isothermal interface depth increases.

4.2.2. The comparison of the temperature field near the interface

Fig. 10 shows non-isothermal phase change hoists the interfacial position and increases the variational gradient of interfacial temperature. Fig. 11 depicts the isothermal lines drill through the phase change interface in the non-isothermal phase change while the isothermal line is superposing with the interface in the isothermal phase change. The difference of both isothermal lines in the melt domain is obvious. The isothermal lines are smoother in the non-isothermal phase change while in isothermal phase change they are hoisted from the left to the right and are concaved towards the crystal. It is because the phase change temperature near the centerline is lower than that on the sidewall in the

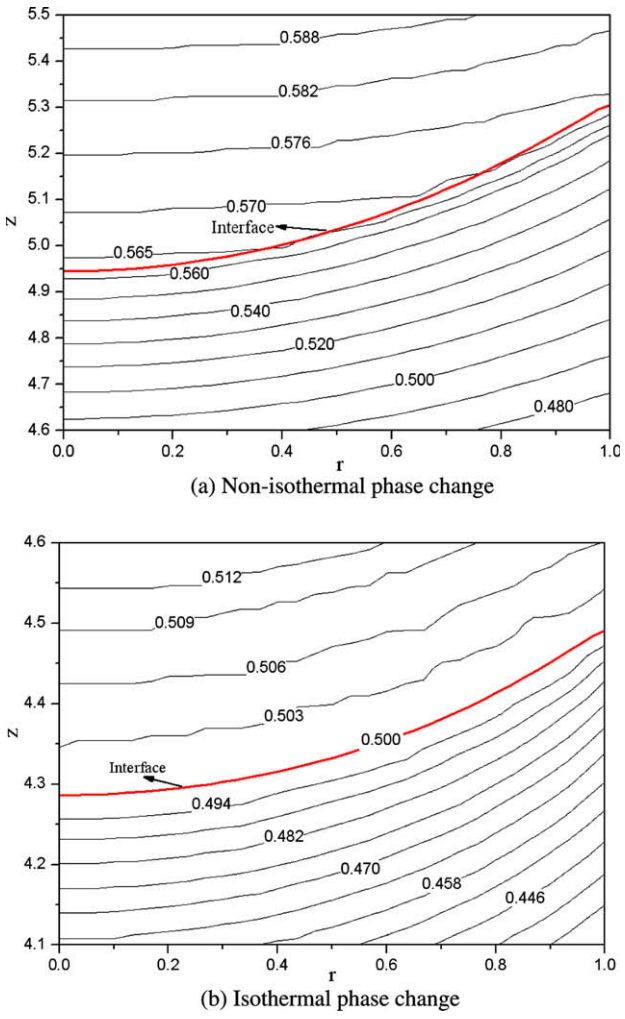

Fig. 11. The comparison of the temperature field near the interface between the non-isothermal and isothermal phase change.

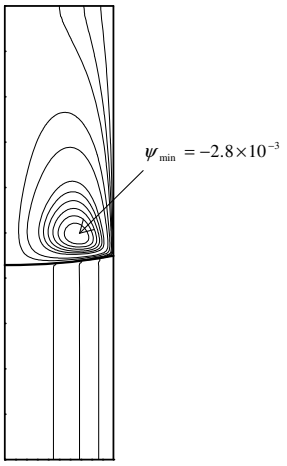

Fig. 12. The flow field in the isothermal phase change.

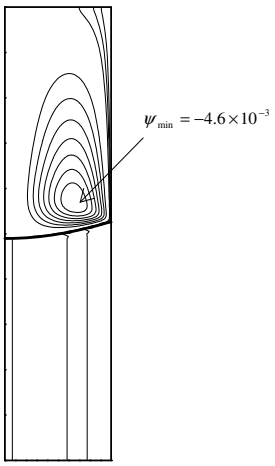

Fig. 13. The flow field with the double-diffusive convection in the non-isothermal phase change.

non-isothermal phase change. Along the isothermal lines drilled through the interface, a large quantity of latent heat is released in the neighborhood of the centerline while the phase change does not occur near the wall, so that the temperature near the centerline in the melt of the non-isothermal phase change becomes higher and the isothermal lines go smoother.

4.2.3. The comparison of the flow

Fig. 12 shows that the absolute value of the stream function in the center of the vortex in the isothermal phase change is greater than that in the non-isothermal phase change (see Fig. 4(a)). This means the flow is weakened by the non-isothermal phase change process.

4.3. Effects of double-diffusive convection in the melt on the non-isothermal phenomena

Double-diffusive convection is formed due to the combination of temperature and concentration gradients in the fluid, in which the flow was driven by the thermal and solutal buoyance forces simultaneously.

4.3.1. The comparison between the natural convection and the double-diffusive convection

Fig. 13 shows the flow field of the double-diffusive convection ($Gr_S = -1.0 \times 10^5$, $Gr_T = 1.0 \times 10^6$) in the non-isothermal phase change. Comparing with the natural convection (see Fig. 4(a), $Gr_S = 0$, $Gr_T = 1.0 \times 10^6$), it can be seen that a vortex occurs in both cases because of the thermal gradient on the wall. But the absolute value of the stream function in the center of the vortex in the double-diffusive convection is greater than that in the natural convection. This means the thermally induced convection is enhanced by the solutal convection.

As shown in Fig. 14, the interfacial position and the temperature with the convection including the natural convection and the double-diffusive convection near the centerline and the wall is lower than these without flow. The reason is that the convection enhances the heat and mass transfer, so that reduces the local temperature and affects the interfacial shape. Since the flow and the transfer of heat and mass are enhanced by solutal buoyancy in the double-diffusive convection (see Fig. 13), therefore, the interfacial position and the melting temperature in the case of double-diffusive convection become lower than these in the case of natural convection.

4.3.2. Effects of the solutal Grashof number

In Fig. 15, the absolute value of vertical velocity in most part of the melt at the centerline ($r = 0$) and near the wall ($r = 0.9$) increases as the absolute value of Gr_S increases.

Fig. 16 shows the interface shape and melting temperature both moves downward near the centerline and the wall as the absolute value of the solutal Grashof number increases.

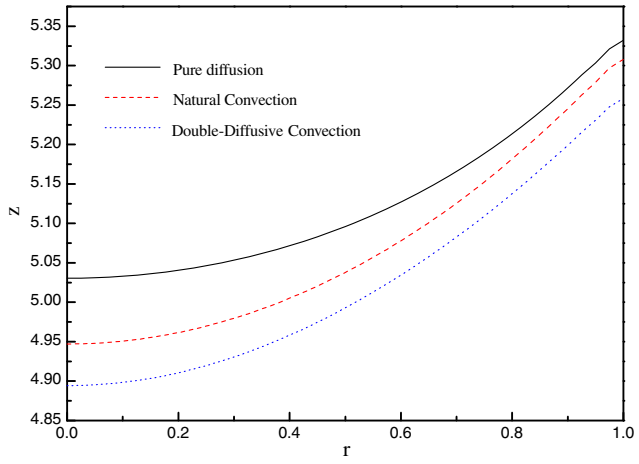

(a) The interface shape

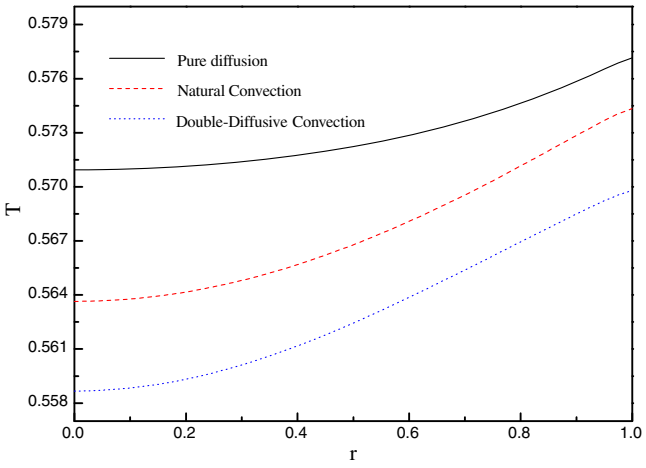

(b) The melting temperature

Fig. 14. The comparison of the interfacial characteristics among the pure diffusion, the natural convection and the double-diffusive convection in the non-isothermal phase change.

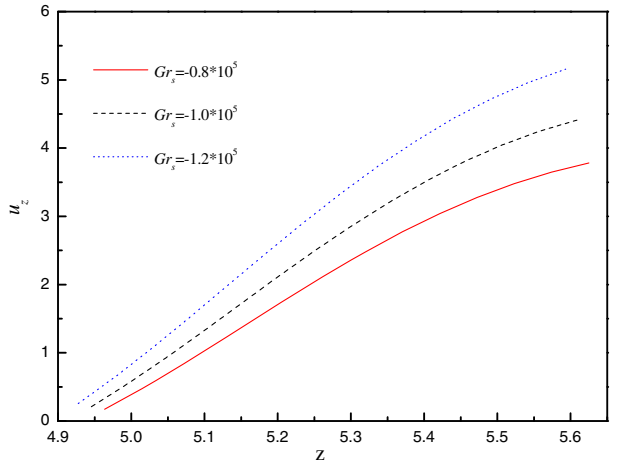

(a) $r = 0$

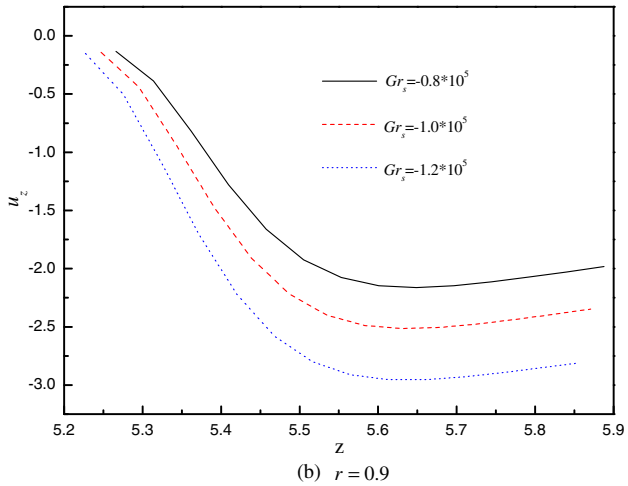

(b) $r = 0.9$

Fig. 15. The variation of vertical velocity with axial position at location $r = 0$ (a) and $r = 0.9$ (b) in the melt in the non-isothermal phase change.

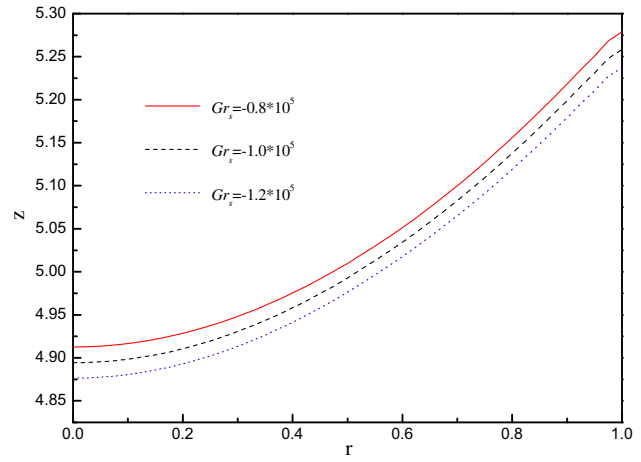

(a) The interface shape

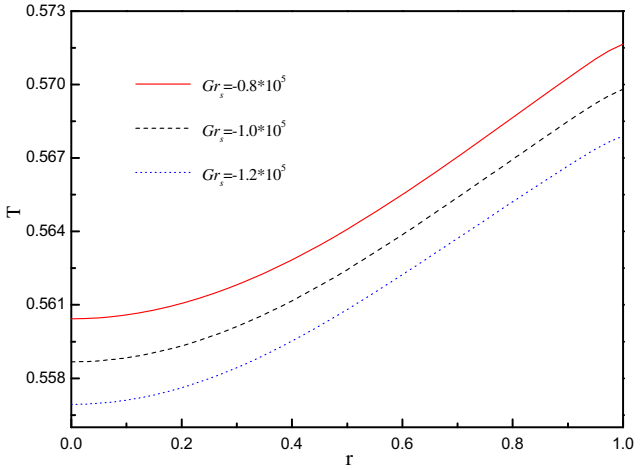

(b) The melting temperature

Fig. 16. Effects of Gr_S on the interface shape (a) and the melting temperature (b) at the interface in the non-isothermal phase change.

5. Conclusions

Numerical simulations were conducted to investigate the non-isothermal phase change phenomena while using the vertical Bridgman method to grow HgCdTe crystals. For the given conditions, the main conclusions are as follows:

(1) During the steady growth region of the HgCdTe crystal growth using VBM, the phase change interface is concave towards the crystal, and has obvious two-dimensional non-isothermal phase change character, that is, the melting temperature near the sidewall is relatively higher than that near the centerline.

(2) The influence of the growth parameters such as *Bi*, *Ste*, *U* and the flow parameters including Gr_T and Gr_S all affect the interfacial characteristics. Variations of *Bi* and *Ste* lead to obvious changes of the interface shape, but the melting temperature at the interface have few variations. Variations of Gr_T and Gr_S lead to obvious changes of the melting temperature, but the interface shape have few variations. The interface shape and the melting temperature are both strongly affected by *U*.

(3) Comparing with isothermal phase change, the non-isothermal phase change hoists the interfacial position and increases the variational gradient of interfacial temperature. The isothermal lines drill through the phase change interface in the non-isothermal phase change. The isothermal lines in the melt become more planar than those in the crystal. The interface depth becomes greater in the non-isothermal phase change, so that is far away from the desired planar shape and does harm to the crystal quality.

(4) The thermally induced convection is enhanced by the solutal induced convection. The interfacial positions and the temperatures near the centerline with flow (natural convection and double-diffusive convection) are lower than these without flow. The interfacial position and temperature in the double-diffusive convection become lower than these in the natural convection. This shows the double-diffusive convection affects non-isothermal phase-change process and produces different interfacial characteristics.

Acknowledgement

This work was supported by the National Natural Science Foundation of China (Grant No. 50336040).

References

[1] D.A. Watring, S.L. Lehoczky, Magneto-hydrodynamic damping of convection during vertical Bridgman–Stockbarger growth of HgCdTe, J. Cryst. Growth 167 (3–4) (1996) 478–487.
[2] X.H. Liu, W.Q. Jie, Y.H. Zhou, Numerical analysis on HgCdTe growth by ACRT-VBM, J. Cryst. Growth 209 (4) (2000) 751–762.
[3] X.H. Liu, W.Q. Jie, Y.H. Zhou, Numerical analysis on $Cd_{1-x}Zn_xTe$ growth by ACRT-VBM, J. Cryst. Growth 219 (1–2) (2000) 22–31.
[4] S.Z. Xiao, S.P. Shao, Bridgman growth of $Hg_{1-x}Cd_xTe$ using ACRT, Laser Infrared 27 (1–2) (1997) 301–304.
[5] W.Q. Jie, The shift of the growth interface during the Bridgman process due to the solute redistribution, J. Cryst. Growth 219 (3–4) (2000) 379–384.
[6] J.C. Brice, P. Capper, The phase diagram of the pseudo-binary system CdTe–HgTe and the segregation of CdTe, J. Cryst. Growth 75 (1986) 395–399.
[7] P. Capper, J.J.G. Gosney, et al., Quenching studies in Bridgman-grown $Cd_xHg_{1-x}Te$, J. Cryst. Growth 63 (1983) 154–164.
[8] Y. Wang, Q.B. Li, et al., Effects of growth speed on shape of solid–liquid interface during modified-Bridgman growth of HgCdTe, J. Synth. Cryst. 29 (2002) 45–50.
[9] O. Hong, S. Wei, Numerical simulation of CdTe vertical Bridgman growth, J. Cryst. Growth 173 (1997) 352–366.
[10] C.W. Lan, C.C. Ting, Numerical investigation on the batch characteristics of liquid encapsulated vertical Bridgman crystal growth, J. Cryst. Growth 149 (1995) 175–186.
[11] Y.C. Liu, W.C. Chen, Influence of the gravity on interface shape during crystal growth of LICAF, Sci. China A 30 (1) (2000) 79–87.
[12] Y.F. Wei, W.Z. Fang, et al., Numerical simulation of CdTe growth with vertical Bridgman method, Chin. J. Semiconduct. 22 (7) (2001) 853–859.
[13] C.A. Wang, A.F. Witt, J.R. Carruthers, Analysis of crystal growth characteristics in a conventional vertical Bridgman configuration, J. Cryst. Growth 66 (2) (1984) 299–308.
[14] E.D. Bourret, J.J. Derby, R.A. Brown, Dynamics of Bridgman–Stockbarger growth of non-dilute binary alloys, J. Cryst. Growth 71 (3) (1985) 587–596.
[15] J.J. Derby, R.A. Brown, A fully implicit method for simulation of the one-dimensional solidification of the one-dimensional solidification of a binary alloy, J. Cryst. Growth 41 (1) (1986) 37–46.
[16] E.D. Bourret, J.J. Derby, R.A. Brown, et al., Segregation effects during growth of pseudo-binary systems with large liquidus–solidus separation, Acta Astronaut. 11 (3–4) (1984) 163–171.
[17] Y. Wang, Q.B. Li, Q.L. Han, et al., The choice of the initial velocity of HgCdTe crystal growth using VBM, Infrared Tech. 22 (1) (2000) 25–28.
[18] A. Yeckel, J.J. Derby, Buoyance and rotation in small-scale vertical Bridgman growth of cadmium zinc telluride using accelerated crucible rotation, J. Cryst. Growth 233 (2001) 599–608.
[19] Y. Kawaguchi, H. Yasuda, Y. Okano, et al., Numerical simulation of crystal growth of CdZnTe by vertical gradient freezing method – crucible rotation effect, Int. J. Transport Phenom. 7 (5) (2005) 175–187.
[20] K.F. Shi, J. Liu, W.Q. Lu, Numerical investigation of the interfacial characteristics during Bridgman growth of compound crystals, Appl. Therm. Eng. 27 (2007) 1960–1966.
[21] J. Liu, W.Q. Lu, Numerical simulation of non-isothermal phase change problem using a DRBEM with augmented items, J. Eng. Thermophys. 21 (1) (2006) 85–87.
[22] J. Liu, W.Q. Lu, Preliminary study of non-isothermal phase change phenomena in vertical Bridgman crystal growth, Chin. Sci. Bull. 52 (5) (2007) 701–710.
[23] D.H. Kim, R.A. Brown, Modelling of the dynamics of HgCdTe growth by the vertical Bridgman method, J. Cryst. Growth 114 (1991) 411–434.
[24] H.M. Ettouney, R.A. Brown, Finite-element methods for steady solidification problems, J. Comput. Phys. 49 (1983) 118–150.